International Journal of Statistics and Applied Mathematics

ISSN: 2456-1452 NAAS Rating (2025): 4.49 Maths 2025; 10(6): 236-250 © 2025 Stats & Maths https://www.mathsjournal.com Received: 14-05-2025 Accepted: 10-06-2025

Meena Kumari

Research Scholar, Department of Physical Sciences (Mathematics), Baba Mastnath University, Rohtak, Haryana, India

Sangeeta Malik

Professor, Department of Physical Sciences (Mathematics), Baba Mastnath University, Rohtak, Haryana, India

Dalip Singh

Professor, Department of Physical Sciences (Mathematics), Baba Mastnath University, Rohtak, Haryana, India

Baljit Singh Punia

Assistant Professor, Government College, Barwala, Hisar, Haryana, India

Corresponding Author: Baljit Singh Punia Assistant Professor, Government College, Barwala, Hisar, Haryana, India

Reflection of plane waves in a double poroelastic diffusive medium with microtemperatures and temperature dependent properties

Meena Kumari, Sangeeta Malik, Dalip Singh and Baljit Singh Punia

DOI: https://www.doi.org/10.22271/maths.2025.v10.i6c.2175

Abstract

Purpose: Present analysis is concerned with the reflection of time harmonic plane waves in a homogeneous, isotropic, thermoelastic diffusive medium under the effects of double porosity, microtemperatures and temperature dependent properties.

Methods: Six kinds of coupled longitudinal waves in addition to shear wave and microtemperature wave travel with distinct speeds in such type of medium. Taking into account appropriate boundary constraints, the reflection phenomena is investigated at the stress free surface of the medium.

Results: The expressions of amplitude ratios and energy ratios for the reflected plane waves are obtained. Numerical computations, performed using MATLAB software, analyze the impacts of double porosity, diffusion, temperature dependent properties and microtemperature parameters on the amplitude ratios.

Conclusion: It is observed that the maximum amount of energy goes along the reflected longitudinal displacement wave corresponding to the reflection coefficient |Z1|. Thus, the reflected longitudinal displacement wave is the most dominating wave after reflection as it suppresses the other reflected waves. The computational results are visualized and interpreted through graphs. Notably, it is confirmed that there is no dissipation of energy during the reflection phenomena.

Keywords: Thermoelasticity, reflection, diffusion, double porosity, microtemperatures, temperature dependent properties

Introduction

The theory of thermoelasticity with microtemperatures has received a lot of attention because of its application in the field of continuum mechanics. The theory of microtemperatures deals with the propagation of the temperature wave in a rigid heat conductor which permits the variation of thermal properties at a microstructure level. In accordance with the concept of microtemperatures, each microelement of a thermoelastic solid has a different temperature and relies homogeneously on the microcoordinates of the microelements. Grot [1] introduced the theory of thermodynamics of elastic bodies with microstructure, whose molecules possess microtemperatures. The Clausius-Duhem inequality is modified to include microtemperatures and the first-order moment of energy equations are added to the usual balance laws of a continuum with microtemperatures. Riha [2] developed a model for the heat conduction in materials with microtemperatures. The linear theory of thermoelasticity with microtemperatures was established by Iesan and Quintanilla [3], which was the simplest thermoelastic theory of elastic solids that took into account the microtemperature variables by modifying the Clausius-Duhem inequality. Kalkal et al. [4] investigated the two dimensional thermo-mechanical interactions in a thermodiffusive material with microtemperatures and magnetic field. Deswal et al. [5] examined the reflection phenomenon of plane waves in a homogeneous, isotropic thermoelastic diffusive medium with microtemperatures. Goyal et al. [6] studied the effect of inclined mechanical load on a thermo-diffusive half-space with microtemperatures and microconcentrations.

Material science, petroleum industry, chemical engineering, biomechanics and other fields of engineering rely heavily on porous structures. In recent years, many authors have been interested in the study of the thermoelastic bodies with double porosity structure. The double porosity model demonstrates a double porous structure with macro and micro porosity

connected to body's pores and fissures respectively. By using the classic Darcy's law, Biot [7] presented the first model for a single porosity deformable solid. The Biot theory is based on the concept of compressible constituents and till recently, some of his findings have been utilised as standard references and basis for further investigation in the fields of acoustics, geophysics, and other related ones in the considered body. A non-linear theory of thermoelasticity containing double porous structure was proposed by Iesan and Quintanilla [8]. Kalkal et al. [9] examined the effect of double porosity and gravity in an isotropic, non-homogeneous, functionally graded half-space under three-phase-lag model. Mahato and Biswas [10] studied the two-dimensional problem in a nonlocal thermoelastic medium with double porosity under the purview of Green-Naghdi (III) theory. Othman and Mansour [11] investigated the influence of diffusion and gravity on a thermoelastic medium with double porosity in the context of Lord-Shulman theory.

Diffusion is the passive movement of particles from regions of higher concentration to the regions of lower concentration until equilibrium is reached. It occurs as a result of second law of thermodynamics which states that the entropy or disorder of any system must always increase with time. There is now a great deal of interest in the study of this phenomenon, due to its many applications in geophysics and industrial applications. The thermodiffusion process also helps investigation in the field associated with the advent of semiconductor devices and the advancement microelectronics. By using coupled thermoelastic model, Nowacki [12-14] suggested the theory of thermoelastic diffusion, predicting infinite velocities of propagation for thermoelastic signals. Sherief et al. [15] extended this theory to study the interactions among the processes of elasticity, heat and diffusion in elastic solids that allow for finite speed of propagation of thermoelastic and diffusive waves. Kalkal et al. [16] presented a study on wave propagation in an anisotropic magnetothermoelastic diffusive half space with temperature dependent properties in the context of Green-Lindsay theory. Propagation of plane waves in a magnetothermoelastic medium under the effects of variable thermal conductivity and mass diffusivity is examined by Deswal et al. [17]. Malik et al. [18] studied the reflection and transmission phenomena of plane waves at the interface of two distinct nonlocal generalized thermoelastic solid with diffusion. Said and Othman [19] discussed the two-dimensional problem of a nonlocal thermoelastic diffusion solid with gravity in the context of different theories. By using normal mode technique, Eraki et al. [20] examined the Thomson effect on the behavior of a diffusive magneto-thermoelastic medium with initial stress under dual-phase-lag model.

The prime objective of the current study is to investigate the reflection phenomenon of plane waves in a double poroelastic diffusive medium under the effect of microtemperatures and temperature dependent properties. A lot of research has been carried out in recent years on double poroelastic medium, but the work in its present form has not been studied by any researcher till now. It has been detected that there are six sets of coupled longitudinal waves, one set of transverse wave and one set of independent microtemperature wave propagating with different speeds in the considered medium. The amplitude ratios of these reflected waves have been calculated numerically and their variations with the angle of incidence are depicted graphically. Energy partitioning among reflected waves at the free boundary has also been calculated and various interesting results have been discussed. It has been

verified that during reflection phenomena, the sum of energy ratios is equal to unity at each angle of incidence. Some comparisons have been made in figures to estimate the influence of double porosity, diffusion, temperature dependent properties and microtemperatures parameters.

2. Governing equations

Following Kansal ^[21, 22], the constitutive relations and field equations in a homogeneous isotropic double poroelastic diffusive medium with microtemperature can be written as: Constitutive equations

$$\sigma_{ij} = 2\mu e_{ij} + (\lambda e \not - _1T \not - _2C + b\phi + d\psi)\delta_{ij}$$

$$\varepsilon = -be - \alpha_1\phi - \alpha_3\psi + \gamma_1T + m_1C,$$

$$\zeta = -de - \alpha_3\phi - \alpha_2\psi + \gamma_2T + m_2C,$$

$$\sigma_i = \alpha\phi_{,i} + b_1\psi_{,i} - r_1w_i,$$

$$\chi_i = b_1\phi_{,i} + \gamma\psi_{,i} - r_2w_i,$$

$$q_i = K^*T_{,i} + s_1w_i,$$

$$q_{ij} = -s_4w_{r,r}\delta_{ij} - s_5w_{i,j} - s_6w_{j,i},$$

$$Q_i = (s_1 - s_2)w_i + (K^* - s_3)T_{,i},$$

$$e_{ij} = \frac{1}{2}(u_{i,j} + u_{j,i}).$$

Equation of motion

$$\mu \nabla 2ui + (\lambda + \mu)\nabla e - \beta 1\nabla T - \beta 2\nabla C + b\nabla \phi + d\nabla \psi = \rho u^{"}i.$$

Equilibrated stress equations of motion

$$\alpha \nabla 2 \varphi + b \mathbf{1} \nabla 2 \psi - b e - \alpha \mathbf{1} \varphi - \alpha \mathbf{3} \psi + \gamma \mathbf{1} \mathbf{T} + m \mathbf{1} \mathbf{C} - r \mathbf{1} \nabla w \mathbf{i} = K \mathbf{1} \varphi$$
,"

$$b1\nabla 2\phi + \gamma \nabla 2\psi - de - \alpha 3\phi - \alpha 2\psi + \gamma 2T + m2C - r2\nabla wi = K2\psi.$$

Equation of first moment of energy

s6wi,jj + (s4 + s5)wj,ij - s2wi - s3T,i - r3w`i - r1
$$\nabla\phi$$
 - r2 $\nabla\psi$ = 0.

Heat conduction equation

 $K*T,ii + s1wi,i = \beta1T0e^{\cdot} + \rho CeT^{\cdot} + acT0C^{\cdot} + \gamma1T0\phi^{\cdot} + \gamma2T0\psi^{\cdot}$

Equation of mass diffusion

$$C' = Dc[bc\nabla 2C - ac\nabla 2T - \beta 2\nabla 2e - m1\nabla 2\varphi - m2\nabla 2\psi]. \quad (15)$$

porous material, si(i=1,2,...,6) are constant constitutive coefficients, $\beta 1 = (3\lambda + 2\mu)\alpha t$, at is the thermal expansion coefficient, $\beta 2 = (3\lambda + 2\mu)\alpha c$, ac is the diffusion expansion coefficient, T = T * - T0, T * is absolute temperature, T0 is reference temperature of the medium in its natural state assumed to be is the non-equilibrium concentration, C0 is the mass concentration at natural state, t is time, ϕ and ψ are volume fraction fields related to pores and fissures respectively, ρ is the mass density, K* is the coefficient of thermal conductivity, Ce is the specific heat at constant strain, ac is measure of thermodiffusion effect, Dc is the thermoelastic diffusion constant, bc is measure of diffusive effect, K1 and K2 are the equilibrated inertia coefficients.

Our motive is to investigate the effect of the temperature-dependent elastic and thermal moduli on the different physical parameters. Following Noda [23], we assume that

 $\begin{array}{l} (\mu,\lambda,\beta1,\beta2,b,d,\alpha,b1,\gamma,\alpha1,\alpha2,\alpha3,\gamma1,\gamma2,ac,bc,m1,m2,r1,r2,r3,K1,\\ K2,s1,s2,\ s3,\ s4,\ s5,\ s6) = (\mu0,\ \lambda0,\ \beta10,\ \beta20,\ b0,\ d0,\ \alpha0,\ b01,\\ \gamma0,\ \alpha10,\ \alpha20,\ \alpha30,\ \gamma10,\ \gamma20,\ a0c,\ bc0,\ m01,\ m02,\ r10,\ r20,\\ r30,\ K10,\ K20,\ s01,\ s02,\ s30,\ s04,\ s05,\ s06)f(T0), \end{array}$

Where f(T0) is a given non-dimensional function of temperature such that $f(T0) = (1 - \alpha * T0)$ and $\alpha *$ is an empirical material constant.

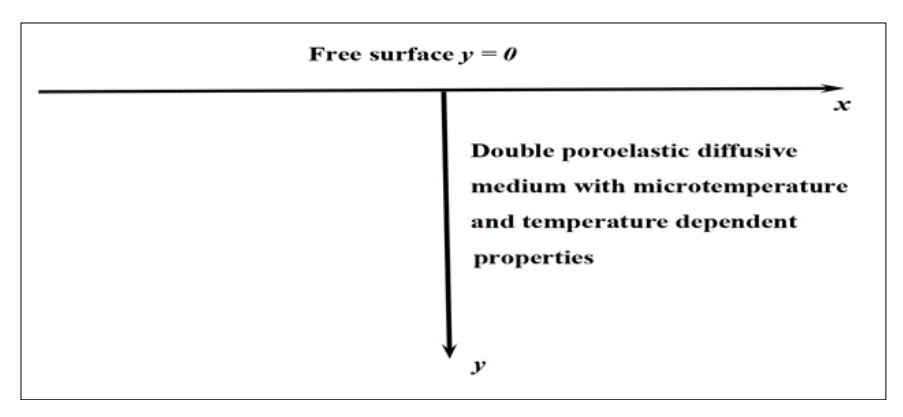


Fig 1: Geometry of the problem

3 Formulation of the problem

Consider a homogeneous, isotropic, double poroelastic, diffusive half-space with microtemperatures and temperature dependent properties. We choose the rectangular cartesian coordinate system (x,y,z) having the surface of the half-space as the plane y=0, with y-axis pointing vertically downwards into the medium so that the half-space occupies the region $y \ge 0$ as shown in Figure 1. The current investigation is restricted to xy-plane and thus all the physical quantities will be functions of the space variables x,y and time t.

Under these considerations, we may write the displacement vector and microtemperature vector as

$$\sim$$
u = (u,v,0), u = u(x,y,t), v = v(x,y,t) w \sim = (w1,w2,0), w1 = w1(x,y,t), w2 = w2(x,y,t). (17)

Taking into consideration (1), (4), (5) and (7) along with the expression (16), the requisite non-zero stress components can be expressed as:

$$\sigma_{yy} = z_1 [(2\mu' + \lambda') \frac{\partial v}{\partial y} + \lambda' \frac{\partial u}{\partial x} + \beta' {}_1T + \beta' {}_2C + b'\phi + d'\psi]$$

$$\sigma_{yx} = z_1 [\mu' (\frac{\partial u}{\partial y} + \frac{\partial v}{\partial x})],$$

$$\sigma_y = z_1 [\alpha' \frac{\partial \phi}{\partial y} + b'_1 \frac{\partial \psi}{\partial y} - r'_1 w_2],$$

$$\chi_y = z_1 [b'_1 \frac{\partial \phi}{\partial y} + \gamma' \frac{\partial \psi}{\partial y} - r'_2 w_2],$$

$$q_{yy} = z_1 [-s'_4 (\frac{\partial w_1}{\partial x} + \frac{\partial w_2}{\partial y}) - s'_5 \frac{\partial w_2}{\partial y} - s'_6 \frac{\partial w_2}{\partial x}],$$

$$q_{yx} = z_1 [-s'_5 \frac{\partial w_2}{\partial x} - s'_6 \frac{\partial w_1}{\partial y}],$$

Where $z1 = 1 - \alpha *T0$. Taking into consideration (16), the governing equations (10)-(15) for two-dimensional problem take the form:

$$(\lambda' + 2\mu') \frac{\partial^2 u}{\partial x^2} + (\lambda' + \mu') \frac{\partial^2 v}{\partial x \partial y} + \mu' \frac{\partial^2 u}{\partial y^2} - \frac{\partial^2 u}{\partial x} + \frac{\partial^2 u}{\partial x^2} + \frac{\partial^2 u}{\partial x^2} + \frac{\partial^2 u}{\partial x^2} + \frac{\partial^2 u}{\partial x^2} - \frac{\partial^2 u}{\partial x^2} + \frac{\partial^2 u}{\partial y} + \frac{\partial^2 u}{\partial y} + \frac{\partial^2 u}{\partial x^2} + \frac{\partial^2 v}{\partial x^2} - \frac{\partial^2 v}{\partial x^2} + \frac{\partial^2 v}{\partial y} + \frac{\partial^2 v}{\partial y$$

International Journal of Statistics and Applied Mathematics

$$\begin{split} s_6' \nabla^2 w_1 + (s_4' + s_5') \big(\frac{\partial^2 w_1}{\partial x^2} + \frac{\partial^2 w_2}{\partial x \partial y} \big) - s_2' w_1 - s_3' \frac{\partial T}{\partial x} - r_3' \frac{\partial w_1}{\partial t} \\ - r_1' \frac{\partial^2 \phi}{\partial t \partial x} - r_2' \frac{\partial^2 \psi}{\partial t \partial x} = 0 \end{split}$$

$$\begin{split} s_6' \nabla^2 w_2 + (s_4' + s_5') \big(\frac{\partial^2 w_1}{\partial x \partial y} + \frac{\partial^2 w_2}{\partial y^2} \big) - s_2' w_2 - s_3' \frac{\partial T}{\partial y} - r_3' \frac{\partial w_2}{\partial t} \\ - r_1' \frac{\partial^2 \phi}{\partial t \partial y} - r_2' \frac{\partial^2 \psi}{\partial t \partial y} = 0 \end{split}$$

$$\frac{\partial C}{\partial t} = z_1 D_c [b' \nabla^2 C - a' \nabla^2 T + \beta \frac{'}{2} \nabla^2 e - m_1' \nabla^2 \phi - m_2' \nabla^2 \psi]$$

Where $\nabla^2=rac{\partial^2}{\partial x^2}+rac{\partial^2}{\partial y^2}$ is the Laplacian operator.

For convenience, we will make use of the following nondimensional variables to normalize the above relations

$$\begin{split} &(x',y',u',v') = \frac{w_0}{c_0}(x,y,u,v), \quad t' = w_0t, \quad (\sigma_i',\chi_i') = \frac{c_0}{\alpha'w_0}(\sigma_i,\chi_i) \\ &(\phi',\psi') = \frac{K_1'w_0^2}{\alpha_1'}(\phi,\psi), \quad \sigma_{ij}' = \frac{1}{\beta_1'T_0}\sigma_{ij}, \quad q_{ij}' = \frac{w_0}{\mu'c_0^2}q_{ij}', \\ &T' = \frac{\beta_1'}{\lambda' + 2\mu'}T, \quad C' = \frac{\beta_2'}{\lambda' + 2\mu'}C, \quad (w_1',w_2') = \frac{c_0}{w_0}(w_1,w_2), \end{split}$$

Where

$$c_0^2 = \frac{\lambda' + 2\mu'}{\rho}, \quad w_0 = \frac{\rho C_e c_0^2}{K^*}$$

Helmholtz decomposition representation of displacement vector \sim u in terms of scalar potential function $\phi 1(x,y,t)$ and vector potential function $U\sim(x,y,t)$ gives:

$$\sim \mathbf{u} = \nabla \omega \mathbf{1} + \nabla \times \mathbf{U} \sim \nabla \cdot \mathbf{U} \sim 0.$$
 (33)

So the displacement components u and v for the twodimensional problem are expressed in terms of these potentials by the following relations:

$$u = \frac{\partial \phi_1}{\partial x} + \frac{\partial \psi_1}{\partial y}, \ v = \frac{\partial \phi_1}{\partial y} - \frac{\partial \psi_1}{\partial x}, \ \vec{U} = (0, 0, \psi_1)$$

The relations connecting microtemperature components to the potential functions are

$$w_1 = \frac{\partial q_1}{\partial x} + \frac{\partial q_2}{\partial y}, \ w_2 = \frac{\partial q_1}{\partial y} - \frac{\partial q_2}{\partial x}.$$
 (35)

Inserting the non-dimensional expressions defined in (32) in equations (24)-(31) along with the consideration of relations (34) and (35), we obtain the following set of equations (suppressing the primes for convenience):

$$(\nabla^2 - a_1 \frac{\partial^2}{\partial t^2})\phi_1 - T - C + a_2 \phi + a_3 \psi = 0$$

$$(\nabla^2 - a_4 \frac{\partial^2}{\partial t^2})\psi_1 = 0,$$

$$\nabla^2 \phi_1 + (a_5 \nabla^2 + a_6 + a_7 \frac{\partial^2}{\partial t^2}) \phi + (a_8 \nabla^2 + a_9) \psi - a_{10} T - a_{11} C + a_{12} \nabla^2 q_1 = 0$$

$$\nabla^2 \phi_1 + (a_{13}\nabla^2 + a_{14})\phi + (a_{15}\nabla^2 + a_{16} + a_{17}\frac{\partial^2}{\partial t^2})\psi - a_{18}T - a_{19}C + a_{20}\nabla^2 q_1 = 0, (39)$$

$$(a_{21}\nabla^2 - a_{22} - a_{23}\frac{\partial}{\partial t})q_1 - a_{24}T - a_{25}\frac{\partial\phi}{\partial t} - a_{26}\frac{\partial\psi}{\partial t} = 0$$

$$(a_{27}\nabla^2 - a_{22} - a_{23}\frac{\partial}{\partial t})q_2 = 0$$

$$(a_{32}\nabla^2\frac{\partial}{\partial t})\phi + (a_{31}\frac{\partial}{\partial t} - a_{29}\nabla^2)T + a_{33}\frac{\partial}{\partial t}C + a_{34}\frac{\partial}{\partial t}\phi + a_{35}\frac{\partial}{\partial t}\psi - a_{30}\nabla^2q_1 = 0, \quad (42)$$

$$(a_{28}\nabla^2)\nabla^2\phi_1 + a_{36}\nabla^2T + (a_{37}\frac{\partial}{\partial t} - a_{38}\nabla^2)C + a_{39}\nabla^2\phi + a_{40}\nabla^2\psi = 0$$

Making use of non-dimensional variables, potential functions and microtemperature components described in (32), (34) and (35), the stresses and heat flux moment defined in (18)-(23) along with some simplifications, provide the following relations:

$$\begin{split} \sigma_{yy} &= a_{41} \frac{\partial^2 \phi_1}{\partial y^2} + a_{42} \frac{\partial^2 \phi_1}{\partial x^2} - a_{43} \frac{\partial^2 \psi_1}{\partial x \partial y} - a_{41} T - a_{41} C + a_{44} \phi + a_{45} \psi, \\ \sigma_{yx} &= a_{43} \frac{\partial^2 \phi_1}{\partial x \partial y} + \frac{a_{43}}{2} (\frac{\partial^2}{\partial y^2} - \frac{\partial^2}{\partial x^2}) \psi_1, \\ \sigma_y &= a_{46} \frac{\partial \phi}{\partial y} + a_{47} \frac{\partial \psi}{\partial y} - a_{48} (\frac{\partial q_1}{\partial y} - \frac{\partial q_2}{\partial x}), \\ \chi_y &= a_{47} \frac{\partial \phi}{\partial y} + a_{49} \frac{\partial \psi}{\partial y} - a_{50} (\frac{\partial q_1}{\partial y} - \frac{\partial q_2}{\partial x}), \\ q_{yy} &= a_{51} (\frac{\partial^2}{\partial x^2} + \frac{\partial^2}{\partial y^2}) q_1 - a_{52} (\frac{\partial^2 q_1}{\partial y^2} - \frac{\partial^2 q_2}{\partial x \partial y}), \\ q_{yx} &= -a_{52} \frac{\partial^2 q_1}{\partial x \partial y} + (a_{53} \frac{\partial^2}{\partial x^2} - a_{54} \frac{\partial^2}{\partial y^2}) q_2, \end{split}$$

Where ai(i = 1,2,...,54) are listed in appendix A.

4. Solution of the problem

In order to find the analytic solution of the system of partial differential equations (36)-(43), we suppose the solution of the form:

$$(\phi_1, \psi_1, \phi, \psi, T, C, q_1, q_2)(x, y, t) = (\phi_1, \psi_1, \phi, \psi, T, T, C, q_1, q_2)\exp(ik(x\sin\theta - y\cos\theta) - i\omega t), (50)$$

Where ϕ^-1,ψ^-1,ϕ^- , ψ^- , $T,^-$, $C,^-$, q^-1 and q^-2 are the amplitudes of the reflected waves. k is the wave number, ω is the angular frequency having the definition $\omega = kv$, v being the phase velocity and $(\sin\theta,\cos\theta)$ denotes the projection of wave normal onto the xy- plane.

Substituting from (50), into equations (36)-(43), we obtain the following set of equation

$$(-k2 + f1)\varphi^{-1} - T^{-} - C^{-} + a2\varphi^{-} + a3\psi^{-} = 0,$$
 (51)

$$(-k2 + f2)\psi^{-}1 = 0,$$
 (52)

$$-k2\phi^{-}1 + (f3 - a5k2)\phi^{-} + (a9 - a8k2)\psi^{-} - a10T^{-} - a11C^{-} - a12k2q^{-}1 = 0,$$
 (53)

$$-k2\phi^{-}1 + (a14 - a13k2)\phi^{-} + (f4 - a15k2)\psi^{-} - a18T^{-} - a19C^{-} - a20k2q^{-}1 = 0,$$
 (54)

$$(f5 - a21k2)^{-}q1 - a24T^{-} + f6\phi^{-} + f7\psi^{-} = 0, (55)$$

$$(f8 - a27k2)^{-}g2 = 0$$
, (56)

$$f9k2\phi^-1 + (f10 + a29k2)T^- - f11C^- - f12\phi^- - f13\psi^- + a30k2q^-1 = 0,$$
 (57)

$$f14k4\phi^-1 - a36k2T^- + (f15 + a38k2)C^- - a39k2\phi^- - a40k2\psi^- = 0,$$
 (58)

Where fi(i = 1,2,...,15) are listed in appendix B.

The condition for the existence of a non-trivial solution of the homogeneous system of equations (51), (53)-(55) and (57)-(58) provides us:

$$v12 + A*v10 + B*v8 + C*v6 + D*v4 + E*v2 + F* = 0,$$
 (59)

Where A*,B*,C*,D*,E* and F* are calculated with the help of MATLAB programming.

It is noted that the equation (59) is hexic in v2, whose roots will gives the velocities of six vibrating waves.

From equations (52) and (56), we have

$$v^2 = \frac{\omega^2}{f_2}$$
, (60)

$$v^2 = \frac{a_{27}\omega^2}{f_8}.$$
 (61)

The roots of equation (60) and (61) will give the velocities (v7) and (v8) of transverse displacement wave and an independent microtemperature wave, respectively.

The equation (59) is hexic and (60) and (61) are linear in v2 with complex coefficients, showing that the corresponding waves are attenuated in nature. The complex phase velocity vi(i = 1,2,...,8) of each wave can be resolved into propagation velocity Vi(i = 1,2,...,8) and attenuation coefficient Q-i 1(i = 1,2,...,8). For a longitudinal wave with complex velocity vi = viR + viI, define Vi =(viR2 + viI2)/viR and Q-i 1=-2viI/viR as its phase velocity and attenuation coefficient respectively, where the letters R and I in the subscript denote the real and imaginary parts. The phase speeds of these waves depend upon the frequency ω and wave number k. Hence these waves are found to be dispersive and attenuated in nature.

5. Reflection phenomenon

Here, we shall discuss the reflection phenomenon, when a set of coupled longitudinal waves having amplitude A0 propagating with phase speed V0 and making an angle θ 0 with the normal is made to strike at the free surface y=0. Corresponding to the incident wave, we obtain eight reflected waves as shown in Figure 2. We postulate the following reflected waves to satisfy the boundary conditions at the free plane surface:

- 1. Six sets of coupled longitudinal waves of amplitudes A1,2,...,6 propagating with the speeds V1,2,...,6 and making angles θ1,2,...,6 respectively with the normal.
- 2. A transverse waves of amplitude A7 propagating with speed V7 and making angle θ 7 with the normal.

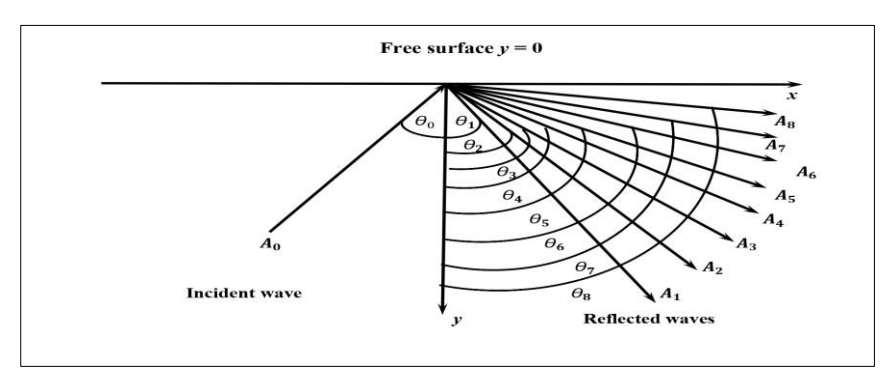


Fig 2: Schematic of the problem

3. An independent microtemperature wave with amplitude A8 propagating with speed V8 and making angle $\theta8$ with the normal.

Therefore, the full structure of the wave field consisting of the incident and reflected waves, can be written as

$$(\phi_1, \phi, \psi, T, C, q_1) = (1, \eta_{11}, \eta_{21}, \eta_{31}, \eta_{41}, \eta_{51}) A_0 P_0^- + \sum_{i=1}^6 (1, \eta_{1i}, \eta_{2i}, \eta_{3i}, \eta_{4i}, \eta_{5i}) A_i P_i^+,$$
(62)
$$\psi_1 = A_7 P_7^+,$$
(63)

$$q_2 = A_8 P_8^+, \quad (64)$$

Where] is the phase factor of the wave incident at an angle $\theta 0$ with amplitude A0, Pi+=exp[\(\pi \left(i(x \sin \theta + y \cos \theta) - \pi \text{wit}]\), (i = 1,2,...,8) are the phase factors of the waves reflected at angles θi with amplitudes Ai. $\eta 1i$, $\eta 2i$, $\eta 3i$, $\eta 4i$, $\eta 5i$ (i = 1,2,...,6) are the coupling parameters among $\phi^- 1$, ϕ , $-\psi$, -T, $-C^-$ and $q^- 1$. The expressions of coupling parameters are given by

$$\eta_{1i} = -\frac{E_{1i}}{E_{2i}}, \quad \eta_{2i} = -\frac{E_{3i} - E_{4i}\eta_{1i}}{E_{5i}}, \quad \eta_{3i} = \frac{-(E_{6i} + E_{7i}\eta_{1i} + E_{8i}\eta_{2i})}{R_{18}}$$

$$\eta_{4i} = -E_{9i} + \eta_{3i} - a_2 \eta_{1i} - a_3 \eta_{2i}, \quad \eta_{5i} = \frac{a_{24} \eta_{3i} - f_6 \eta_{1i} - f_7 \eta_{2i}}{E_{10i}}$$

Where Eji(j = 1,2,...,10) and R18 are listed in appendix C.

6. Boundary conditions

The amplitudes Ai (i = 1,2,...,7) can be determined by imposing suitable boundary conditions at the free surface y=0. Since the boundary of the half-space is adjacent to vacuum, it is free from surface tractions. So, the boundary conditions at the free surface y=0 are described as:

- 1. Vanishing of normal mechanical stress,
- Vanishing of tangential mechanical stress,
- 3. Vanishing of equilibrated stress corresponding to pores,
- Vanishing of equilibrated stress corresponding to fissures,
- 5. Temperature deviation at the free surface is zero,
- 6. Concentration at the free surface is zero.
- 7. Vanishing of normal heat flux moment,
- 8. Vanishing of tangential heat flux moment.

Mathematically, these boundary conditions can be expressed as:

$$\sigma yy = 0$$
, $\sigma yx = 0$, $\sigma y = 0$, $\chi y = 0$, $T = 0$, $C = 0$, $qyy = 0$, $qyx = 0$. (65)

The boundary conditions prescribed above are identically satisfied if and only if $\omega = \omega 1 = \omega 2 = \omega 3 = \omega 4 = \omega 5 = \omega 6 = \omega 7 = \omega 8$ and Snell's law holds, which gives the relation among angles of incidence and reflection as k1 sin θ 0 = k1 sin θ 1 = k2 sin θ 2 = k3 sin θ 3 = k4 sin θ 4 = k5 sin θ 5 = k6 sin θ 6 = k7 sin θ 7 = k8 sin θ 8, which can further be written as (extended Snell's law).

$$\frac{\sin \theta_0}{V_1} = \frac{\sin \theta_1}{V_1} = \frac{\sin \theta_2}{V_2} = \frac{\sin \theta_3}{V_3} = \frac{\sin \theta_4}{V_4} = \frac{\sin \theta_5}{V_5} = \frac{\sin \theta_6}{V_6} = \frac{\sin \theta_7}{V_7} = \frac{\sin \theta_8}{V_8}. \quad (66)$$

From Snell's law (66), we observe that $\theta 0 = \theta 1$, the other angles of reflection depend upon the phase velocities Vi (i = 1,2,...,8) which are functions of material parameters.

Using expressions (62)-(64) in the boundary conditions (after making non-dimensional) given by (65), we obtain a non-homogeneous system of equations as:

$$\sum_{j=1}^{8} b_{ij} Z_j = M_i, \quad (i = 1, 2, ..., 8), \quad (67)$$

Where 8) are the amplitude ratios of the reflected waves. All the elements of the matrix [bij] together with column matrix [Mi] are defined in Appendix D.

7. Energy partitioning

We shall now consider the partitioning of incident energy between different reflected waves at the surface element of unit area. Following Achenbach [24], the instantaneous rate of work of surface traction is the scalar product of the surface traction and the particle velocity. This scalar product is called the power per unit area, denoted by P *, and represents the rate at which the energy is transmitted per unit area of the surface, i.e., the energy flux across the surface element. The time average of P * over a period, denoted by P *, represents the average energy transmission per unit surface area per unit time. Thus, the rate of energy transmission at the surface y = 0 is given by

$$P *= \sigma yyy' + \sigma yxu' + \sigma y\psi' + \gamma y\phi' + qyyw2 + qyxw1.$$
 (68)

Now, we calculate P * for the incident and each of the reflected waves and hence obtain the energy ratios. The energy ratios Ei (i = 1,2,...,8) of the various reflected waves are defined as the ratios of energy corresponding to the reflected waves to the energy of the incident wave. The expressions for these energy ratios Ei (i = 1,2,...,8) for reflected waves are defined as

$$E_i = \frac{\langle P_i^* \rangle}{\langle P_0^* \rangle}, \quad (i = 1, 2, ..., 8), \quad (69)$$

Where the expressions of and are given by $P0* = -\omega k1M1 \cos\theta 0 + \omega k1M2 \sin\theta 0 - \iota \omega M3\eta 21 - \iota \omega M4\eta 11 - \iota k1M7 \cos\theta 0\eta 51 + \iota k1M8 \sin\theta 0\eta 51,$ $Pi* = \omega kib1i \cos\theta i - \omega kib2i \sin\theta i - \iota \omega b3j\eta 2i - \iota \omega b4j\eta 1i + \iota kib7i \cos\theta i\eta 5i - \iota kib8i \sin\theta i\eta 5i, (i = 1,2,...,6)$

$$P_7^* = -b_{17}\omega k_7 \sin\theta_7 + b_{27}\omega k_7 \cos\theta_7$$

$$P_8^* = b_{78} \iota k_8 \sin \theta_8 + b_{88} \iota k_8 \cos \theta_8$$

We note that these energy ratios depend on the elastic properties of the medium, angle of incidence and amplitude ratios. The phenomena of conservation of energy at the surface will be verified graphically in numerical results and discussion section.

8. Special cases

8.1 Without double porosity

To discuss the problem of wave propagation and reflection in a thermoelastic diffusive medium with microtemperatures and temperature dependent properties, it is sufficient to set the value of double porosity parameters $b = d = \alpha = b1 = \gamma = \alpha 1 = \alpha 2 = \alpha 3 = r1 = r2 = \gamma 1 = \gamma 2 = m1 = m2 = 0$ into the constitutive relations and field equations. With these modifications, the corresponding amplitude ratios and energy ratios can be obtained from equations (67) and (69) for the incidence of a set of coupled waves. In addition, if we neglect the influences of temperature dependent property from the medium, then the outcomes coincide with those of Deswal *et al.* ^[5].

8.2 Without microtemperature

If we assume that k1 = k2 = k3 = k4 = k5 = k6 = r1 = r2 = r3 = 0, then we shall deal with a relevant problem of reflection phenomenon in a thermoelastic diffusive half-space with double porosity and temperature dependent property. By taking into consideration the above mentioned modifications, equations (67) and (69) will provide us the reflection coefficients and energy ratios for the corresponding problem. If we also remove the effect of doule porosity from the medium, then the results of the relevant problem coincide with the particular case (Isotropic medium) of Kalkal *et al.* [16] (in the absence of the magnetic field).

8.3 Without temperature dependent property

The effect of temperature dependent property can be removed from the medium by taking $\alpha * = 0$ in the governing equations. If we further remove the impact of double porosity, then our results match with those of Sheoran *et al.* [25] in the absence of magnetic field, rotation and initial stress.

9 Numerical results and discussion

In order to discuss the problem in greater details and to find out the nature of dependence of reflection coefficients and energy ratios on the angle of incidence and material parameters, a numerical analysis is carried out with the help of computer programming using the software MATLAB. For the purpose of numerical computation, the material constants of the problem are taken from Sherief and Saleh [26] $\lambda 0 = 7.76 \times 1010 \text{Nm}{-2}, \ \mu 0 = 3.86 \times 1010 \text{Nm}{-2}, \ \rho = 8954 \text{kgm}{-3}, \ T0 = 293 \text{K}, Ce = 3831 \text{m2s}{-2} \text{K}{-1}, Dc = 0.85 \times 10{-8} \text{kgsm}{-3}, \ \alpha t = 1.78 \times 10{-5} \text{K}{-1}, \ \alpha c = 1.2 \times 10{-4} \text{m3kg}{-1}, \ a0c = 1.2 \times 10{4} \text{m2K}{-1} \text{s}{-2}, \ b0c = 0.9 \times 104 \text{m5kg}{-1} \text{s}{-2},$

$$K* = 386Wm-1K-1$$
.

The double porosity parameters are taken from Khalili [27] b0 = $0.9 \times 104 Nm-2$, $d0 = 0.1 \times 104 Nm-2$, $b10 = 1.2 \times 10-6N$, $\alpha0 = 1.3 \times 10-5N$, $\alpha10 = 2.3 \times 1010 Nm-2$, $\alpha20 = 2.4 \times 1010 Nm-2$, $\alpha30 = 2.5 \times 1010 Nm-2$, $\gamma0 = 1.1 \times 10-5N$, $\gamma10 = 0.16 \times 105 Nm-2$, $\gamma20 = 0.219 \times 105 Nm-2$, $m10 = 2.9 \times 1012 N$, $m02 = 2.9 \times 1010 N$, $K10 = 0.1456 \times 10-12 Nm-2s2$, $K20 = 0.1546 \times 10-12 Nm-2s2$.

The values of microtemperature parameters are taken from Sheoran *et al.* $^{[25]}$ k10 = 0.0035Ns-1, k20 = 0.0045Ns-1, k30 = 0.0055Ns-1K-1, k40 = 0.065Ns-1m-2, k50 =

0.076Ns-1m-2, k60 = 0.096Ns-1m-2, r10 = 0.0085N, r20 = 0.0085N, $r30 = 0.15 \times 10$ -9N.

For the purpose of numerical computation, we also consider angular velocity $\omega = 0.001$ and a* = 0.005.

Considering the above physical data, we have evaluated the amplitude ratios, energy ratios and sum of modulus of energy ratios for each value of angle of incidence varying from normal incidence to grazing incidence for incident wave propagating with speed V0. With the help of abovementioned constants, the numerical results are obtained and presented graphically.

The presentation is divided into five categories for convenience:

Category 1: In this category (Figures 3(a)-(h)), the amplitude ratios Zi(i = 1,2,...,8) have been evaluated at different angles of incidence of a coupled longitudinal wave for different values of double porosity parameter (solid line), 1.6 × 10-6 (dashed line), (dotted line). The variation in amplitude ratio |Z1| corresponding to an incident longitudinal wave versus angle of incidence $\theta 0$ is depicted in Figure 3(a). It can be observed that the amplitude ratio |Z1| has its maximum value unity at normal incidence, it then decreases with increase in θ 0 till θ 0 = 520 and thereafter, it increases with an increase in θ 0 for three different values of discussed above. An increase in the value of double porosity parameter results in an increase in the absolute numerical values of the reflection coefficient |Z1|, which illuminates the fact that the is having an increasing effect on the profile of the reflection coefficient |Z1|. Figure 3(b) depicts the effect of double porosity parameter on the profile of reflection coefficient |Z2|, for three different values mentioned above. Increase in the value of results in increase in numerical values of reflection coefficient |Z2|, which illuminates the fact that the double porosity parameter is having a noticeable increasing effect on the profile of reflection coefficient |Z2|.

The influence of double porosity parameter on the profile of amplitude ratio |Z3| is depicted in figure 3(c). By comparing the three solution curves, it is observed that the modulus values of amplitude ratio |Z3| are lesser for greater value of Hence double porosity parameter has a decreasing effect on the profile of this amplitude ratio |Z3|. In figure 3(d), we have elucidated the variations of amplitude ratio |Z4| against the angle of incidence. It can be noticed from the plot that the values of |Z4| increase monotonically in the interval $00 < \theta 0 \le$ 550 and then decrease as $\theta 0$ increases further. Double porosity coefficient b1 is having an increasing influence on the amplitude ratio |Z4|. In figure 3(e), a similar pattern of distribution of amplitude ratio |Z5| is observed for the three distinct values of the double porosity parameter. The figure shows that an increase in the value of reduces the values of |Z5|. The variations of amplitude ratios |Z6|, |Z7| and |Z8| versus angle of incidence are depicted in figures 3(f), 3(g) and 3(h) respectively, for three different values of mentioned above. From the figures, one can notice that the values of amplitude ratios |Z6|, |Z7| and |Z8| increase with an increase in the value of double porosity parameter. Thus, double porosity parameter has an increasing effect on the profile of amplitude ratios |Z6|, |Z7| and |Z8|.

Category 2: In this category, figures 4((a)-(h)) are drawn to show the variations in the absolute values of the amplitude ratios |Zi| (i = 1,2,...,8) with the angle of incidence, for different values of the diffusion parameter (solid line), 1.5×104 (dashed line), 1.8×104 (dotted line) when a coupled

wave is made incident at the free surface y = 0. Figure 4(a) represents the variation in the value of reflection coefficient |Z1| with the angle of incidence for three different values of diffusion parameter. As shown in figure, the value of reflection coefficient |Z1| lies near to unity for the entire range of angle of incidence and is showing negligible effect of diffusion parameter. The variations of amplitude ratios |Z2| and |Z3| versus angle of incidence are depicted in figures 4(b) and 4(c) respectively, for different values of the diffusion parameter. It can be seen from these figures that the variation pattern of reflection coefficients |Z2| and |Z3| is almost similar for all the three values of The increase in the value of results in the decrease in numerical values of reflection coefficients |Z2| and |Z3|, which illuminates the fact that the diffusion parameter is having a noticeable decreasing effect on the profile of reflection coefficients |Z2| and |Z3|.

Figures 4(d) and 4(e) present the variations of absolute values of amplitude ratios |Z4| and |Z5| respectively against the angle of incidence for the three different values of diffusion parameter mentioned above. It can be concluded from the plots that diffusion parameter is having a decreasing influence on the amplitude ratios |Z4| and |Z5|. In figure 4(f), we have elucidated the variations of amplitude ratio |Z6| against the angle of incidence. It can be noticed from the plot that the values of |Z6| increase monotonically in the interval $00 < \theta 0 \le$ 550 and then decrease as $\theta 0$ increases further. Diffusion parameter is having an increasing influence on the amplitude ratio |Z6|. Figures 4(g) and 4(h) are plotted to show the variations of reflection coefficients |Z7| and |Z8| respectively, for different values of the diffusion parameter. Both of these reflection coefficients decrease with an increment in the value of diffusion parameter and show a similar pattern of variations.

Category 3: In this category, figures 5(a)-5(h) are plotted to demonstrate the effect of temperature dependent property parameter α * on the profile of reflection coefficients |Zi| (i = 1,2,....8). In this figure, the solid line and dashed line refer to the presence ($\alpha * = 0.005$) and absence (($\alpha * = 0$) of temperature dependent property respectively. In figure 5(a) the modulus values of amplitude ratio Z1 are computed against the angle of incidence for two different cases: in presence and absence of temperature dependent property. The figure reveals that the reflection coefficient |Z1| has qualitatively similar behaviour for both the cases and presence of temperature dependent property decreases the numerical values of amplitude ratio |Z1|. In figure 5(b), we have elucidated the variation of amplitude ratio |Z2| against the angle of incidence. The presence of temperature dependent property acts to decrease the magnitude of amplitude ratio |Z2| in the whole range of angle of incidence. The variations of amplitude ratios |Z3|, |Z4| and |Z5| versus angle of incidence are depicted in figures 5(c), 5(d) and 5(e) respectively, for with and without temperature dependent property. It can be noticed from the figures that in presence of temperature dependent property parameter, the magnitude of amplitude ratios |Z3|, |Z4| and |Z5| is greater as compared to in absence of temperature dependent property parameter. Figures 5(f), 5(g) and 5(h) manifest the effect of temperature dependent property parameter on the profiles of reflection coefficients |Z6|, |Z7| and |Z8| respectively. It is evident from the plots that the presence of temperature dependent property parameter decreases the values of |Z6|, |Z7| and |Z8|, hence indicating a decreasing effect on amplitude ratio |Z6|, |Z7| and |Z8|.

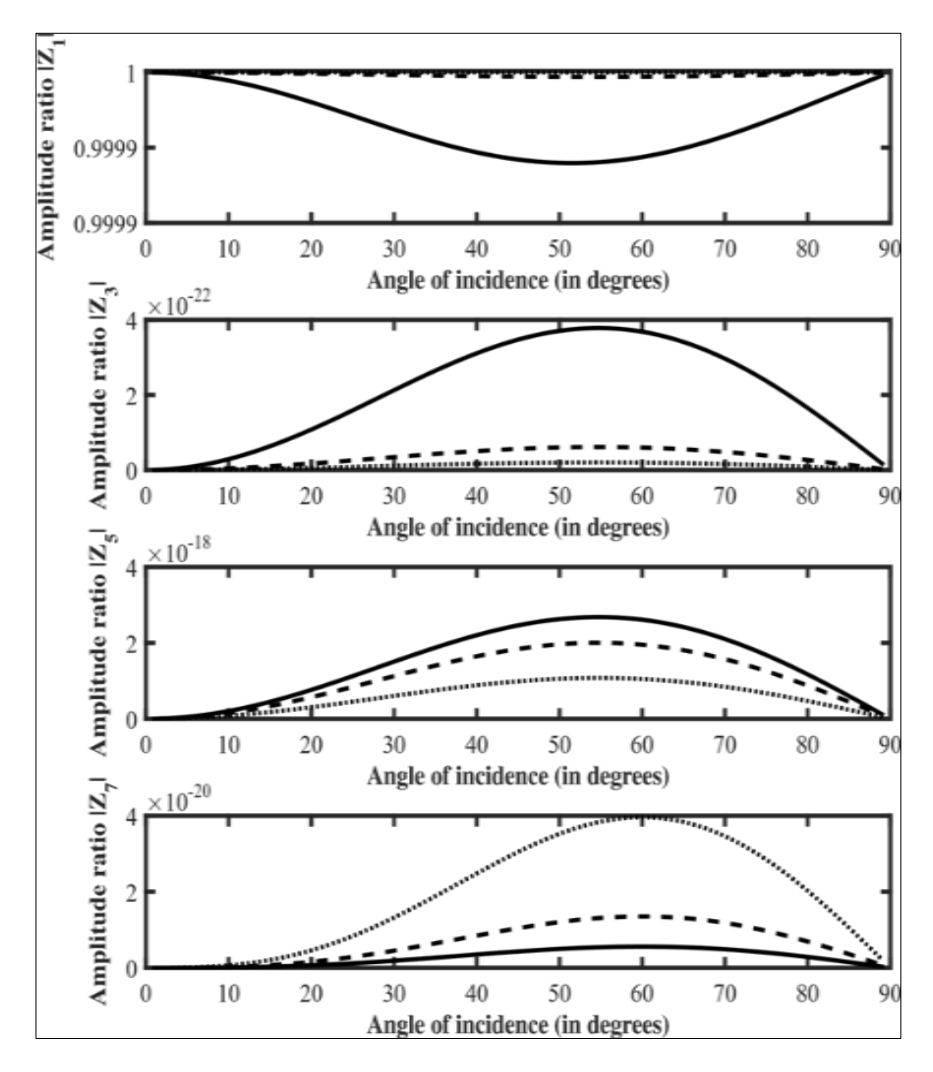
Category 4: In this category, the values of reflection coefficients |Zi| (i = 1,2,...,8) have been computed at different angles of incidence for three different values of microtemperature parameter r3: r3 = $1.5 \times 10-8$ (solid line), $r3 = 2.5 \times 10-8$ (dashed line), $r3 = 3.5 \times 10-8$ (dotted line) and are shown in figures 6(a)-6(f). The variation in reflection coefficient |Z1| corresponding to an incident wave against angle of incidence $\theta 0$ is displayed in figure 6(a). From the plot, we notice that there is an increasing influence of microtemperature parameter r3 on the profile of amplitude ratio |Z1|. Figure 6(b) depicts the effect of microtemperature parameter on the profile of reflection coefficient |Z2|, for three different values mentioned above. Increase in the value of r3 results in decrease in numerical values of reflection coefficient |Z2|, which illuminates the fact that the microtemperature parameter is having a noticeable decreasing effect on the profile of reflection coefficient |Z2|. A similar effect of microtemperature parameter is observed on the profiles of reflection coefficients |Z3| and |Z4| in figures 6(c) and 6(d). However, |Z3| and |Z4| attain small numerical values in comparison to |Z2|. Figures 6(e) and 6(f) displays the variation in the reflection coefficient |Z5| and |Z6| with the angle of incidence.

It can be noticed from the figures that the microtemperature parameter has a decreasing effect on the profile of the reflection coefficients |Z5| and |Z6|. It is also noticed from the figures 6(g) and 6(h) that the values of the solution curves of

the reflection coefficients |Z7| and |Z8| against the angle of incidence decrease with an increase in the value of the microtemperature parameter.

Category 5

Category 5 includes figure 7 which depicts the variations of modulus of energy ratios of reflected waves with the angle of incidence of coupled longitudinal wave propagating with velocity V0. The energy conversion in different ranges of angle of incidence is clearly noticed. We can see from the plot that the values of |E1| and sum are almost same and equal to unity irrespective of the variations in angle of incidence. The energy ratios |E2|, |E3|, |E4|, |E5|, |E6|, |E7| and |E8| are very small as the amplitude ratios |Z2|, |Z3|, |Z4|, |Z5|, |Z6|, |E7| and |Z8| were found to be small. These energy ratios have been shown by curves II, III, IV, V, VI and VII in the figure after multiplying their original values by 107,1031,104,104,1017,1041 and 1013 respectively. It can be seen from the figure that the energy carried by reflected coupled longitudinal wave propagating with velocity V1 is maximum in comparison to energy carried along with other reflected waves. It is observed that the profiles of the energy ratios versus angle of incidence are qualitatively similar to the corresponding profiles of the reflection coefficients apart from the magnitudes. It has been verified that at each angle of incidence P8i=1 $|Ei| \approx 1$. Thus, we conclude that energy balance law is verified for each angle of incidence.



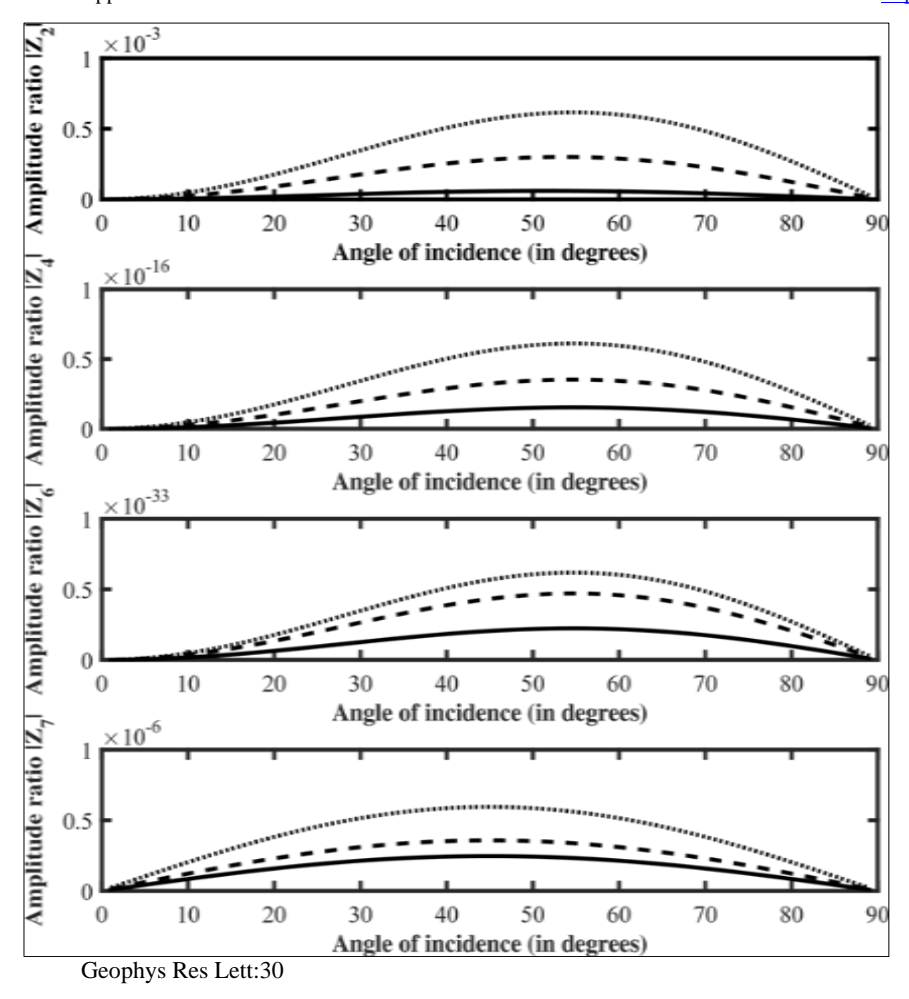
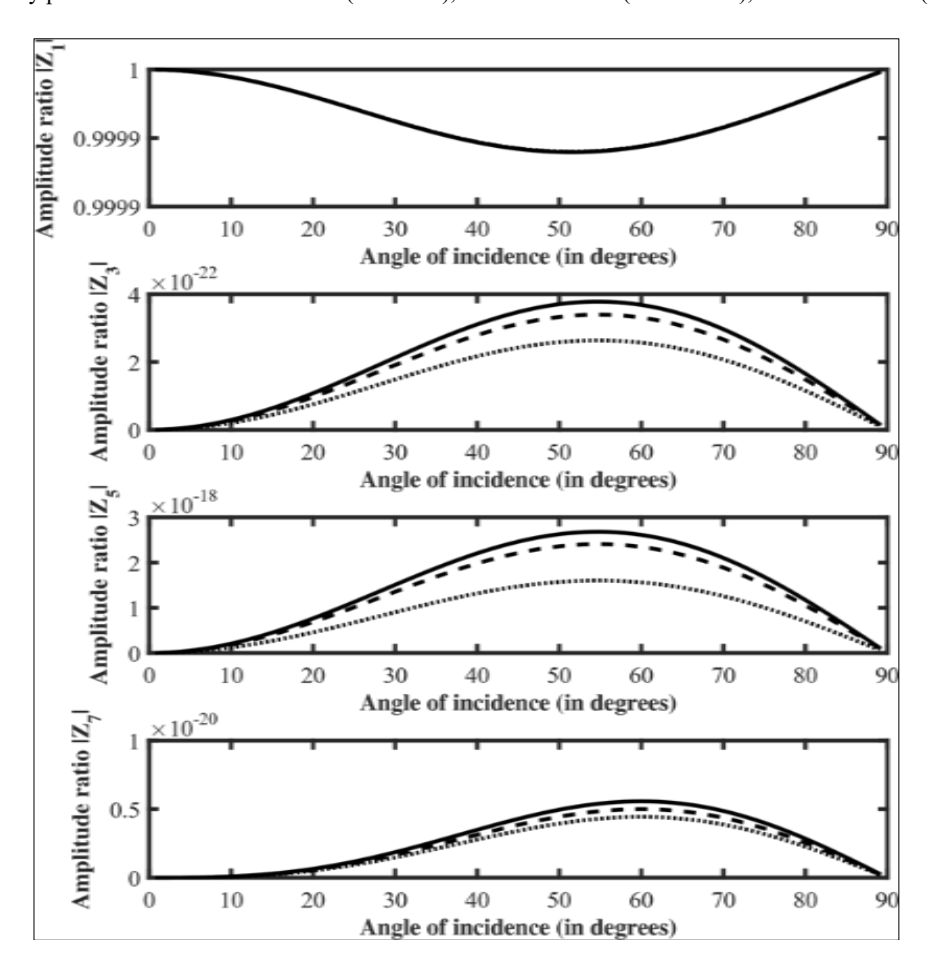


Fig 3: Variations of reflection coefficients |Zi|(i = 1,2,...,8) against angle of incidence of a coupled wave with speed V0 for different values of double porosity parameter b1: b1 = 1.2 × 10-6 (solid line), b1 = 1.6 × 10-6 (dashed line), b1 = 1.8 × 10-6 (dotted line)



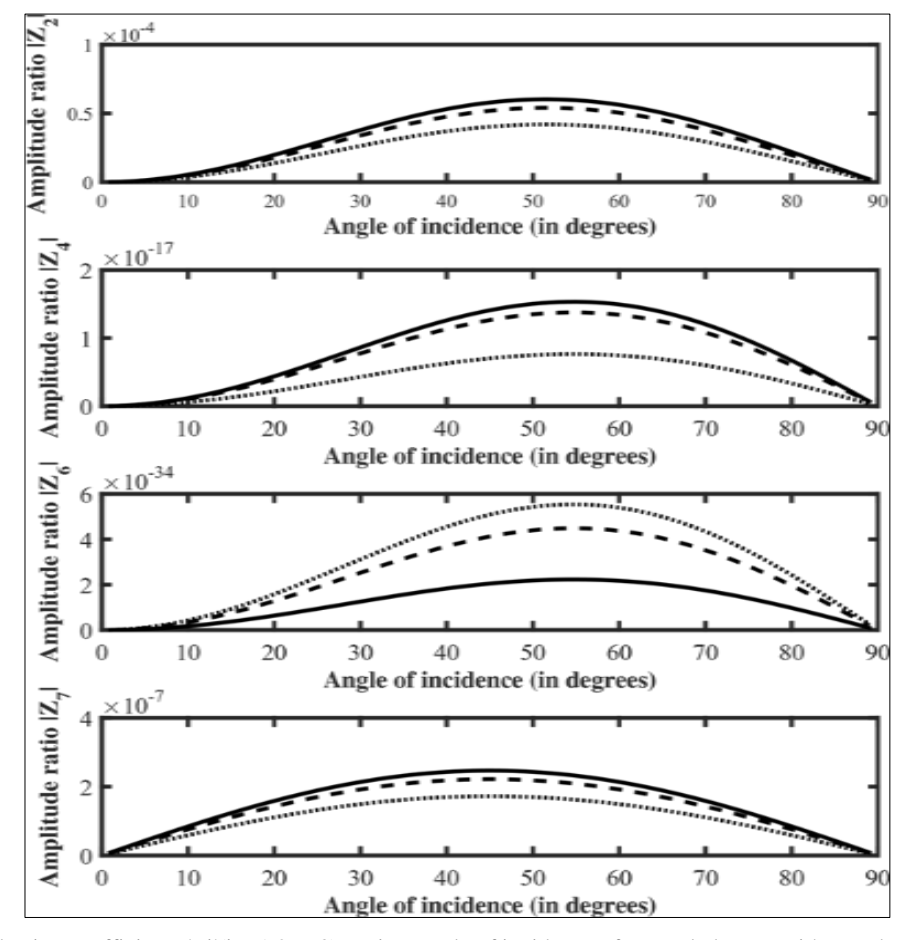
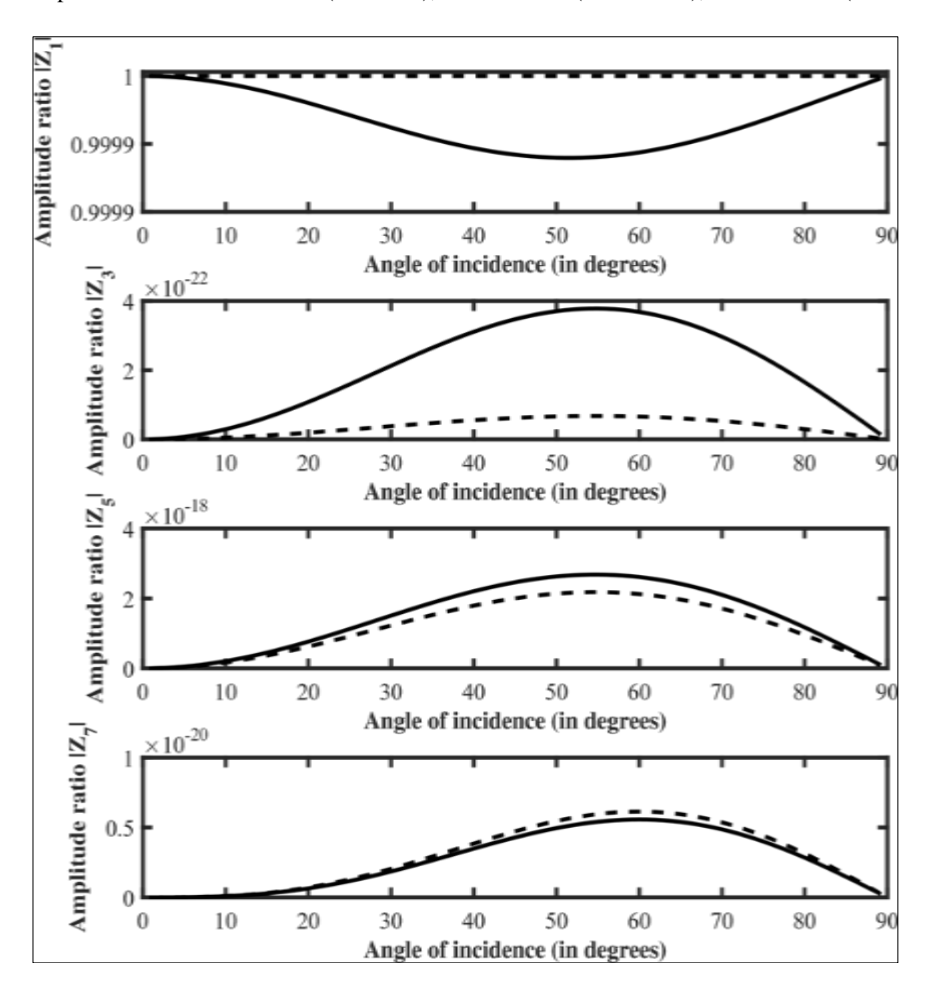


Fig 4: Variations of reflection coefficients |Zi|(i = 1,2,...,8) against angle of incidence of a coupled wave with speed V0 for different values of diffusion parameter ac: ac = 1.2×104 (solid line), ac = 1.5×104 (dashed line), ac = 1.8×104 (dotted line)



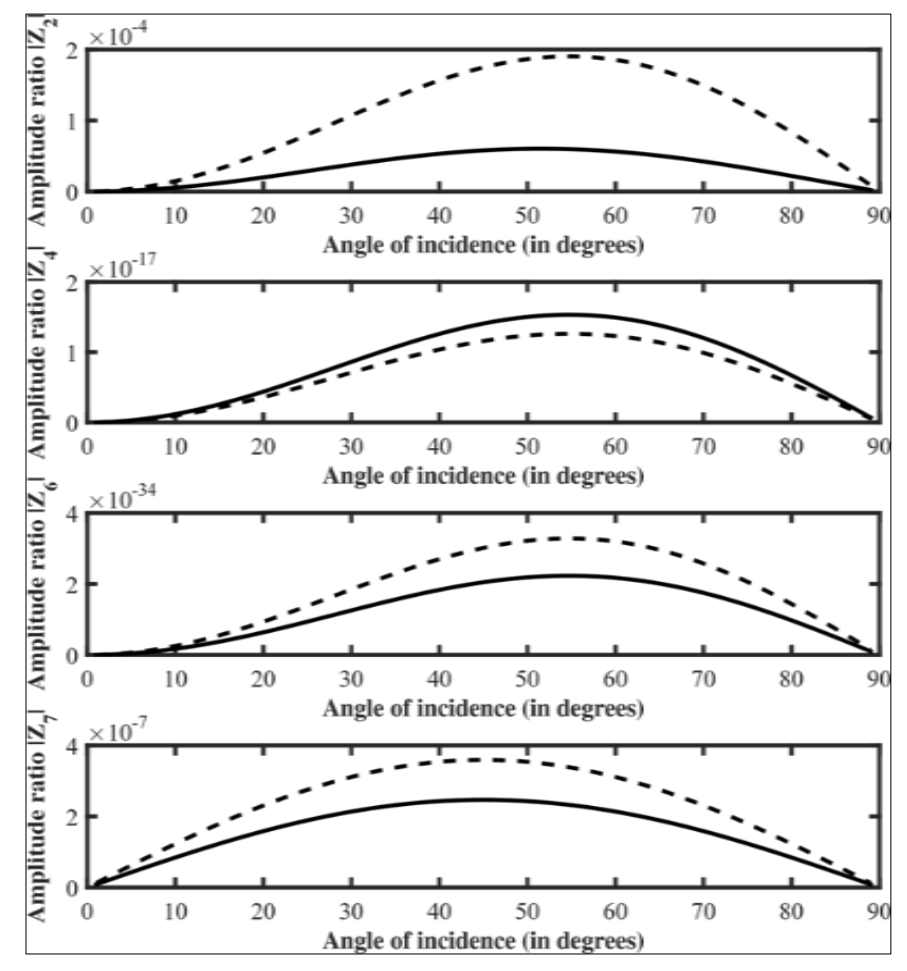
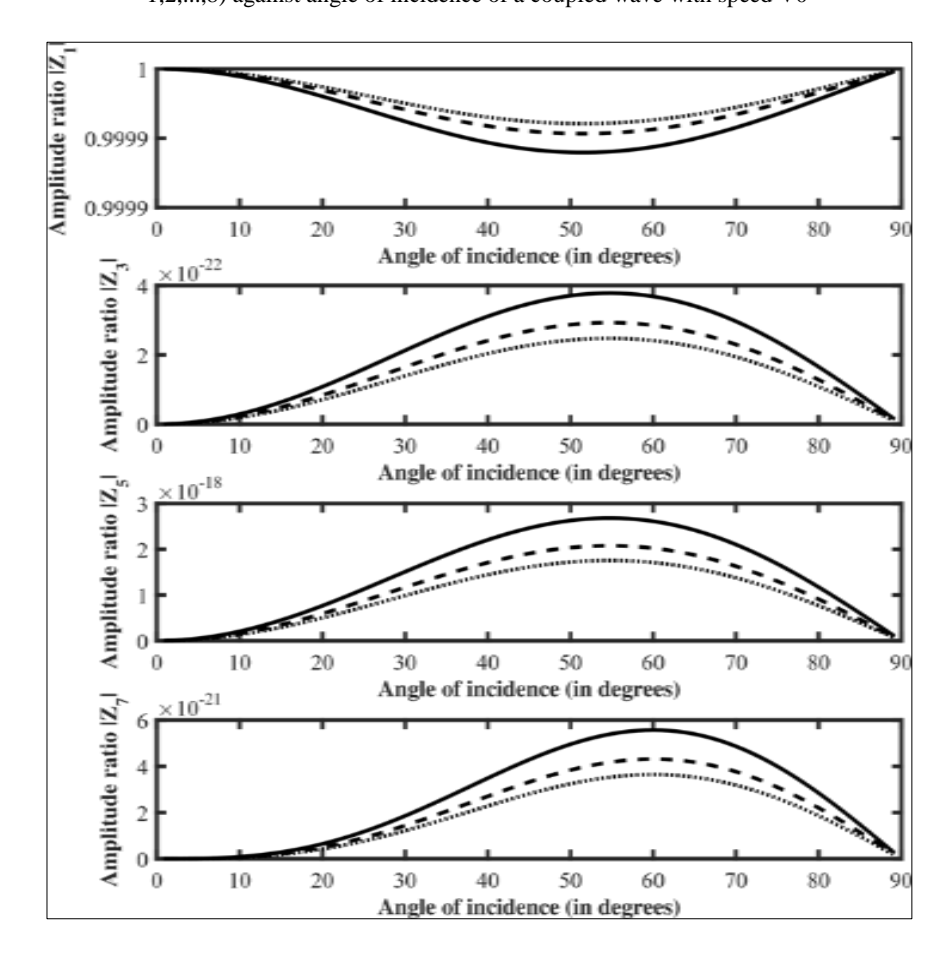


Fig 5: Effect of temperature dependent property parameter $\alpha*$ ($\alpha*$ = 0.005 (solid line), $\alpha*$ = 0 (dashed line)) on the reflection coefficients |Zi|(i = 1,2,...,8) against angle of incidence of a coupled wave with speed V0



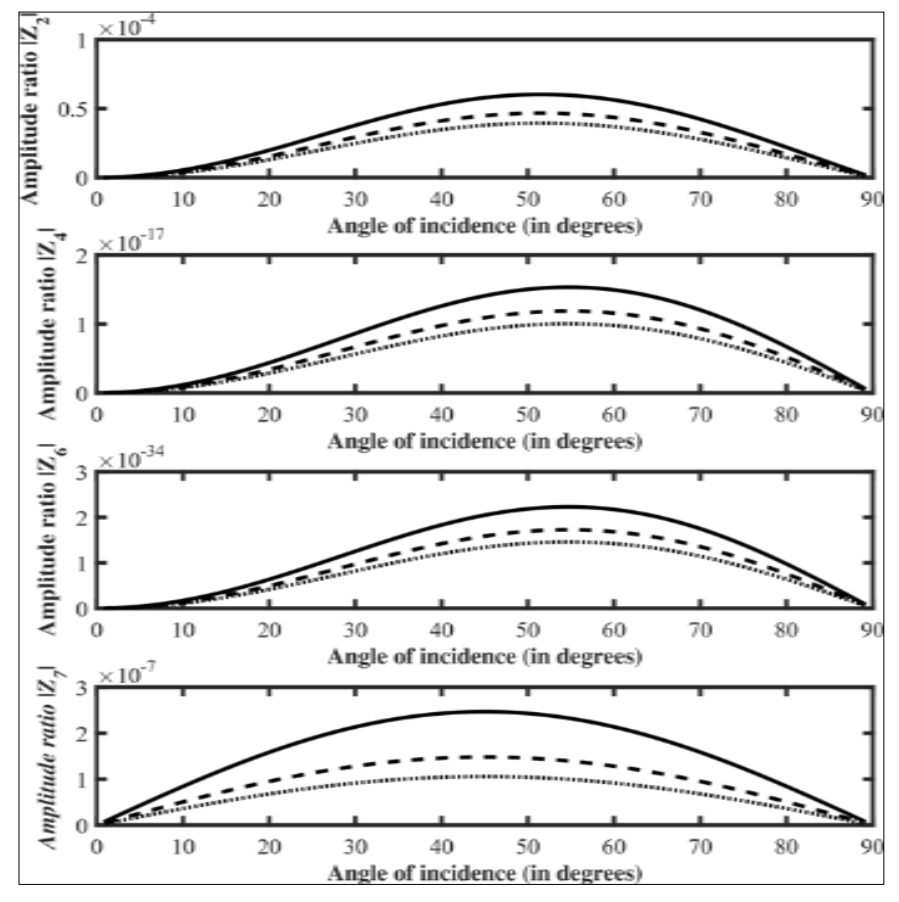


Fig 6: Variations of reflection coefficients |Zi| (i = 1,2,...,8) against angle of incidence of a coupled wave with speed V0 for different values of microtemperature parameter r3: r3 = 1.5 × 10–8 (solid line), r3 = 2.5 × 10–8 (dashed line), r3 = 3.5 × 10–8 (dotted line)

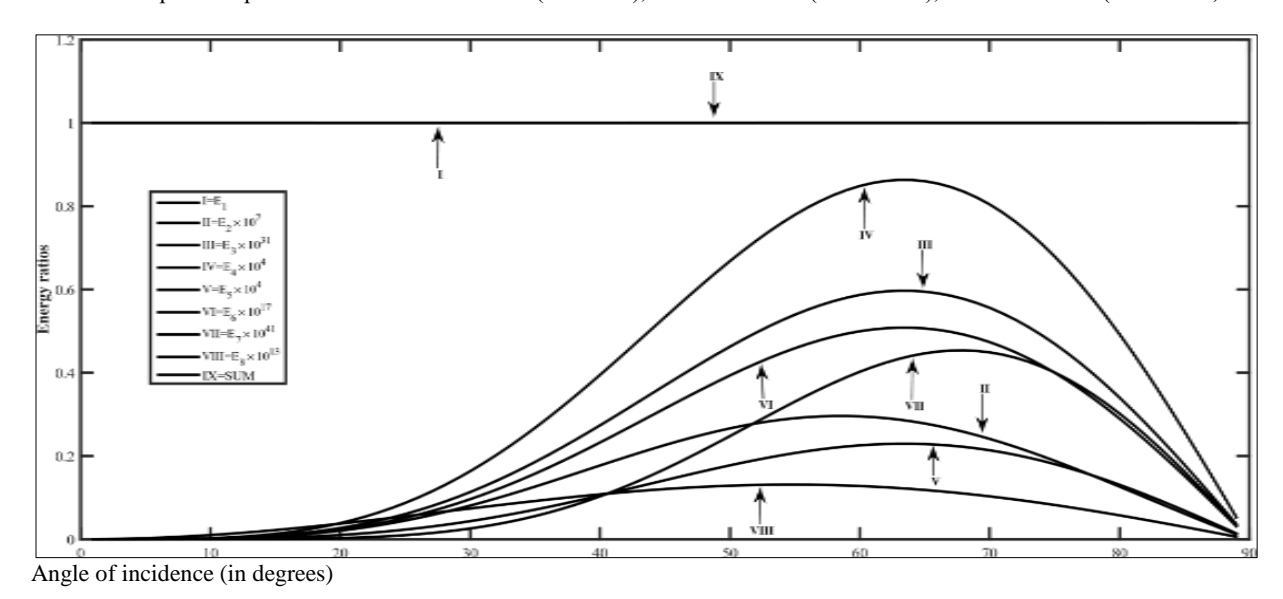


Fig 7: Profile of energy ratios versus angle of incidence.

10 Conclusions

The present study provides a mathematical model to investigate the phenomena of elastic wave propagation from a stress free boundary of a homogeneous isotropic double poroelastic diffusive medium under the effect of microtemperatures and temperature dependent properties. It has been observed that there exist eight plane waves consisting of six sets of coupled longitudinal waves, one set of transverse wave and one set of independent microtemperature wave propagating with distinct speeds. Effects of double porosity, diffusion, temperature dependent properties and microtemperature are discussed numerically and illustrated graphically. The expressions giving the

reflection coefficients and energy ratios have been presented. From the analysis of the illustrations, we can arrive at the following conclusions:

- The reflection coefficients depend on the angle of incidence as well as on the properties of the medium. The nature of this dependency is different for different reflected waves.
- 2. It is observed that all the reflection coefficients |Zi| (i = 1,2,...,8) are highly influenced by the double porosity parameter. It exhibits an increasing effect on the absolute values of the reflection coefficients |Z1|, |Z2|, |Z4|, |Z6|, |Z7| and |Z8| but a decreasing effect is observed on the reflection coefficients |Z3| and |Z5|.

- 3. Theoretical as well as numerical results show that the reflection coefficients of various reflected waves are affected by diffusion coefficient. From the figures, it is noticed that diffusion coefficient has an increasing effect on the profiles of reflection coefficient |Z6| and a decreasing effect is observed on those of |Z2|, |Z3|, |Z4|, |Z5|, |Z7| and |Z8|.
- 4. Effect of temperature dependent property parameter is quite pertinent on the amplitude ratios |Zi| (i=1,2,...,8). The presence of temperature dependent property parameter is having a decreasing effect on the amplitude ratio |Z1|, |Z2|, |Z6|, |Z7| and |Z8| whereas a reverse effect is observed on the profiles of |Z3|, |Z4| and |Z5|.
- 5. All the amplitude ratios |Zi| (i = 1,2,...,8) are highly influenced by microtemperature. A significant increasing impact of microtemperature coefficient is observed on the reflection coefficient |Z1| whereas a reverse effect is observed on the profiles of |Z2|, |Z3|, |Z4|, |Z5|, |Z6|, |Z7| and |Z8|.
- 6. It is observed that the maximum amount of energy goes along the reflected longitudinal displacement wave corresponding to the reflection coefficient |Z1|. Thus, the reflected longitudinal displacement wave is the most dominating wave after reflection as it suppresses the other reflected waves.
- 7. The numerical results show that sum of the modulus values of energy ratios is approximately unity at each angle of incidence. This shows that there is no dissipation of energy during reflection phenomena and hence proving the law of conservation of energy.

11. Applications

The results presented in this article may prove useful for researchers concerned with material science, designers of new materials as well as for those working on the development of hyperbolic thermoelasticity theory. The introduction of double porous structure to the thermoelastic medium has drawn the attention of many engineers, seismologists and scientists due to its application in geophysics, material science, mechanics of bones, drugs, medical devices industry etc. Wave vibration in a thermoelastic solid under the effect of diffusion and microtemperatures with additional parameters like temperature dependent properties gives vital information about the existence of new and modified waves and is of great importance in various technological and geophysical circumstances. Such information may be useful for experimental seismologists/scientists in correcting earthquake estimation. The reflections of seismic waves have a broad range of applications and are primarily used to prospect the geological materials from the Earths interior to provide high-resolution maps. The seismic reflection survey technique builds coherent geological data from the maps of processed seismic reflections. As seismic waves can propagate long distances through the material and gather information from different parts, mapping of stratigraphy as well as structure and significant evaluation of the properties of their constituent materials or components can be accomplished through nondestructive effectiveness of the repair can also be quantified by analyzing the change of wave features before and after repair through nondestructive testing as it uses the feature (velocity, frequency, amplitude, etc.) of elastic waves to estimate the degree of damage.

Conflict of interest disclosure

The authors declare that they have no conflict of interest.

References

- 1. Grot RA. Thermodynamics of a continuum with microstructure. *Int J Eng Sci.* 1969;7:801-814.
- 2. Riha P. On the microcontinuum model of heat conduction in materials with inner structure. *Int J Eng Sci.* 1976:14:529-535.
- 3. Iesan D, Quintanilla R. On a theory of thermoelasticity with microtemperatures. *J Therm Stress*. 2000;23:199-215.
- 4. Kalkal KK, Goyal R, Deswal S. Thermo-mechanical interactions in a magneto-thermoelastic solid with microtemperatures and diffusion. *Microsyst Technol*. 2019;25:3747-63.
- 5. Deswal S, Gunghas A, Kalkal KK. Reflection of plane waves in a thermoelastic diffusive medium under the effect of microtemperatures. *J Therm Stress*. 2019;42(10):1316-29.
- 6. Goyal R, Deswal S, Kalkal KK. Effect of inclined mechanical load on a thermodiffusive half-space with microtemperatures and microconcentrations. *J Vib Eng Technol.* 2024;12:755-71.
- 7. Biot MA. General theory of three-dimensional consolidation. *J Appl Phys.* 1941;12:155-64.
- 8. Iesan D, Quintanilla R. On a theory of thermoelastic materials with a double porosity structure. *J Therm Stress*. 2014;37:1017-36.
- 9. Kalkal KK, Kadian A, Kumar S. Three-phase-lag functionally graded thermoelastic model having double porosity and gravitational effect. *J Ocean Eng Sci.* 2021;8:42-54.
- 10. Mahato CS, Biswas S. State space approach to study thermal shock problem in nonlocal thermoelastic medium with double porosity. *J Therm Stress*. 2023;46:415-43.
- 11. Othman MI, Mansour NT. Effect of relaxation time on generalized double porosity thermoelastic medium with diffusion. *Geomech Eng.* 2023;32:475-82.
- 12. Nowacki W. Dynamic problems of thermoelastic diffusion in solids-I. *Bull Acad Pol Sci, Ser Sci Tech.* 1974;22:55-64.
- 13. Nowacki W. Dynamic problems of thermoelastic diffusion in solids-II. *Bull Acad Pol Sci, Ser Sci Tech.* 1974;22:129-35.
- 14. Nowacki W. Dynamic problems of thermoelastic diffusion in solids-III. *Bull Acad Pol Sci, Ser Sci Tech.* 1974;22:266-75.
- 15. Sherief HH, Hamza FA, Saleh HA. The theory of generalized thermoelastic diffusion. *Int J Eng Sci.* 2004;42:591-608.
- 16. Kalkal KK, Sheokand SK, Deswal S. Reflection of plane waves in an anisotropic magnetothermoelastic diffusive medium with temperature dependent properties. *J Therm Stress*. 2019;42:541-58.
- 17. Deswal S, Jangra A, Punia BS. Reflection of plane waves at the free surface of a magneto-thermoelastic medium with variable thermal conductivity and variable mass diffusivity. *Waves Random Complex Media*. 2022:1-23.
- 18. Malik S, Gupta D, Kumar K, Sharma RK, Jain P. Reflection and transmission of plane waves in nonlocal generalized thermoelastic solid with diffusion. *Mech Solids*. 2023;58:161-88.

- 19. Said SM, Othman MIA. 2D problem of a nonlocal thermoelastic diffusion solid with gravity via three theories. *J Vib Eng Technol*. 2024;12:5423-30.
- 20. Eraki EEM, Fathy RA, Othman MIA. Thomson effect on an initially stressed diffusive magneto-thermoelastic medium via dual-phase-lag model. *J Vib Eng Technol*. 2024;12:6437-48.
- 21. Kansal T. Generalized theory of thermoelastic diffusion with double porosity. *Arch Mech.* 2018;70:241-68.
- 22. Kansal T. The theory of thermoelasticity with double porosity and microtemperatures. *CMST*. 2022;28:87-107.
- 23. Noda N. Thermal stresses in materials with temperature-dependent properties. *Appl Mech Rev.* 1991;44:383-97.

- 24. Achenbach JD. *Wave propagation in elastic solids*. Amsterdam: North Holland; 1973.
- 25. Sheoran D, Kumar S, Kalkal KK. Plane waves in an initially stressed rotating magneto-thermoelastic half-space with diffusion and microtemperatures. *Waves Random Complex Media*. 2022:1-22.
- 26. Sherief HH, Saleh HA. A half space problem in the theory of generalized thermoelastic diffusion. *Int J Solids Struct*. 2005;42:4484-93.
- 27. Khalili N. Coupling effects in double porosity media with deformable matrix. [Details missing].

Appendix A

$$\begin{split} a_1 &= \frac{\rho c_0}{(\lambda' + 2\mu') z_1}, \ a_2 = \frac{b' \alpha_1'}{K_1' w_0^2 (\lambda' + 2\mu')}, \ a_3 = \frac{d' \alpha_1'}{K_1' w_0^2 (\lambda' + 2\mu')}, \ a_4 = \frac{c_0 \rho}{\mu' z_1}, \ a_5 \\ &= \frac{-(\alpha_1)'^2}{b' c_0^2 K_1'}, \ a_6 = \frac{(\alpha_1')^2}{b' w_0^2 K_1'}, \ a_7 = \frac{\alpha_1'}{b'}, \ a_8 = \frac{-b_1' \alpha_1'}{b' c_0^2 K_1'}, \ a_9 = \frac{\alpha_1' \alpha_3'}{b' w_0^2 K_1'}, \ a_{10} = \frac{\gamma_1' (\lambda' + 2\mu')}{b l_1^8 \ '2}, \\ a_{11} &= \frac{m_1' (\lambda' + 2\mu')}{b l_1^8 \ '2}, \ a_{12} = \frac{(r_1')^2 w_0^2}{b' c_0^2}, \ a_{13} = \frac{-b_1' \alpha_1'}{d' w_0^2 K_1'}, \ a_{14} = \frac{\alpha_1' \alpha_3'}{d' w_0^2 K_1'}, \ a_{15} = \frac{-\gamma' \alpha'}{d' c_0^2 K_1'}, \\ a_{16} &= \frac{\alpha_1' \alpha_2'}{d' w_0^2 K_1'}, \ a_{17} = \frac{\alpha' K_2'}{d' K_1'}, \ a_{18} = \frac{\gamma_2' (\lambda' + 2\mu')}{b' k_1'}, \ a_{19} = \frac{m_2' (\lambda' + 2\mu')}{b' k_2'}, \ a_{20} = \frac{r_2' w_0^2}{d' c_0^2}, \\ a_{21} &= (s_4' + s_5' + s_6') \frac{w_0^3}{c_0^3}, \ a_{22} = \frac{s_2' w_0}{c_0}, \ a_{23} = \frac{r_3' w_0^2}{c_0}, \ a_{24} = \frac{s_2' w_0 (\lambda' + 2\mu')}{b' k_1'}, \ a_{25} = \frac{r_1 \alpha_1'}{c_0^2 K_1'}, \\ a_{26} &= \frac{r_2 \alpha_1'}{c_0 K_1'}, \ a_{27} = \frac{s_6' w_0^3}{c_0^3}, \ a_{28} \not\ni \frac{1}{2}, \ a_{29} = \frac{K^* w_0 (\lambda' + 2\mu')}{b' k_2'}, \ a_{30} = \frac{w_0 s_1' z_1}{c_0^2}, \\ a_{31} &= \frac{\rho' C_e (\lambda' + 2\mu')}{\beta_1'}, \ a_{32} \not\ni \frac{1}{2} I_1 T_0, \ a_{33} = \frac{a_c z_1 T_0 (\lambda' + 2\mu')}{b' k_2'}, \ a_{34} = \frac{\alpha_1' \gamma_1' z_1 T_0}{w_0^2 K_1'}, \\ a_{35} &= \frac{\alpha_1' \gamma_2' z_1 T_0}{w_0^2 K_1'}, \ a_{36} &= \frac{a_c (\lambda' + 2\mu')}{\beta_2'}, \ a_{37} &= \frac{c_0^2 (\lambda' + 2\mu')}{z_1 D_c u b_0' \frac{1}{2}}, \ a_{38} &= \frac{b_c (\lambda' + 2\mu')}{\beta_2'}, \\ a_{39} &= \frac{m_1' \alpha_1'}{K_1' w_0^2}, \ a_{40} &= \frac{m_2' \alpha_1'}{K_1' w_0^2}, \ a_{41} &= \frac{z_1 (\lambda' + 2\mu')}{\beta_1' T_0}, \ a_{42} &= \frac{z_1 \lambda'}{\beta_1' T_0}, \ a_{43} &= \frac{z_1 T_1'}{\alpha_1' w_0^2 T_1'}, \\ a_{49} &= \frac{\gamma' \alpha_1' z_1}{\gamma w_0^2 T_0 K_1'}, \ a_{45} &= \frac{z_1 r_2'}{\alpha'}, \ a_{51} &= \frac{-s_4' w_0^3}{\mu' c_0^4}, \ a_{52} &= \frac{(s_4' + s_6') w_0^3}{\mu' c_0^4}, \ a_{53} &= \frac{s_5' w_0^3}{\mu' c_0^4}, \\ a_{54} &= \frac{s_6' w_0^3}{\mu' c_0^4}. \end{aligned}$$

Appendix B

 $\begin{array}{l} f1=a1\omega 2,\ f2=a4\omega 2,\ f3=a6-a7\omega 2,\ f4=a16-a17\omega 2,\ f5=\\ -a22+a23\omega ,\ f6=a25\omega ,\ f7=a26\omega ,\ f8=f5,\ f9=a32\omega ,\ f10\\ =-a31\omega ,\ f11=-a33\omega ,\ f12=-a34\omega ,\ f13=a35\omega ,\ f14=\\ \beta 20,\ f15=-a37\omega . \end{array}$

Appendix C

E1i = R66ki8 + R67ki6 + R68ki4 + R69ki2 + R70, E2i = R71ki8 + R72ki6 + R73ki4+R74ki2 + R75, E3i = R39ki4 + R40ki2 + R41, E4i = R42ki4 + R43ki2 + R44, E5i = R45ki4 + R46ki2 + R47, E6i = R16ki2 + R17, E7i = R19ki2 + R20, E8i = R21ki2 + R22, E9i = -ki2 + f1, E10i = -a21ki2 + f5, i = (1,2,...,6), R1 = 1 - a11, R2 = f1a11, R3 = a10 - a11, R4 = a2a11 - f3, R5 = a3a11 - a9, R6 = 1 - a19, R7 = a19f1, R8 = a18 - a19, R9 = a2a19 - a14, R10 = a3a19 - f4, R11 = -(f9 + f11), R12 = f1f11, R13 = -(f10 + f11), R14 = a2f11 + f12, R15 = a3f11 + f13, R16 = R1a20 - R6a12, R17 = R2a20 - R7a12, R18 = R3a20 - R8a12, R19 = a5a20 - a12a13, R20 = R4a20 - R9a12, R21 = a8a20 - a12a15, R22 = R5a20 - R10a12, R23 = R6a30 + R11a20, R24 = R7a30 + R12a20, R25 = R8a30 + R13a20, R26 = -a20a29, R27 = a13a30, R28 = R9a30 + R14a20, R29 = a15a30, R30 =

R10a30+R15a20, R31 = R1a30 + R11a12, R32 = R2a30 +R12a12, R33 = R13a12, R34 = -a29a12, R35 = a5a30, R36 = R4a30 + R14a12, R37 = a8a30, R38 = R5a30 + R15a12, R39= R16R26, R40 = R16R25 + R17R26 - R18R23, R41 =R17R25 - R24R18, R42 = R19R26, R43 = R19R25 +R20R26 - R18R27, R44 = R20R25 - R18R28, R45 =R21R26, R46 = R22R26 - R18R29, R47 = R22R25 -R18R30, R48 = R16f19 -R18f16, R49 = R17f19 - R16f20 -R17f18, R50 = -R17f20 - R18f18, R51 = R19f19, R52 =R20f19 - R19f20 - R18f21, R53 = -R20f20 - R18f22, R54 =R21f19, R55 = R22f19 - R21f20 - R18f23, R56 = -R22f20 -R18f24, R57 = R16R34, R58 = R17R34 + R16R33 -R18R31, R59 = R17R33 - R18R32, R60 = R19R34, R61 =R19R33 + R20R34 - R18R35, R62 = R33R20 - R18R36, R63 = R21R34, R64 = R21R33 + R22R34 - R18R37, R65 =R33R22, R66 = R48R63 - R54R57, R67 = R49R63 +R48R64 - R54R58 - R55R57, R68 = R50R63 + R49R64 +R48R65 - R54R59 - R55(R58 + R59), R69 = R49 R65 +R64R30 - R55R59 - R56R58, R70 = R50R65 - R56R59, R71 = R51R63 - R60R54, R72 = R49R63 + R48R64 -R54R61 - R55R60, R73 = R53R63 + R52R64 + R51R65 - R54 R62 - R55R61 - R56R60, R74 = R52R65 + R53R64 - R56R61 - R55R62, R75 = R53R65 - R56R62.

Appendix D

b1j = $-a41kj2 \cos 2 \theta j - a42kj2 \sin 2 \theta j - a41\eta 3j - a41\eta 4j + a44\eta 1j + a45\eta 2j$, b17 = $a43k72 \cos \theta 7 \sin \theta 7$, b2j = $-2a43kj2 \cos \theta j \sin \theta j$, b27 = $a43k72(-\cos 2 \theta 7 + \sin 2 \theta 7)$, b3j = $ukj \cos \theta j (-a46\eta 1j - a47\eta 2j + a48\eta 5j)$, b38 = $a48uk8 \sin \theta 8$, b4j = $ukj \cos \theta j (-a47\eta 1j - a49\eta 2j + a50\eta 5j)$, b48 = $a50uk8 \sin \theta 8$, b5j = $ukj \cos \theta j (-a47\eta 1j - a49\eta 2j + a50\eta 5j)$, b48 = $a50uk8 \sin \theta 8$, b5j = $ukj \cos \theta j (-a47\eta 1j - a49\eta 2j + a50\eta 5j)$, b48 = $ukj \cos \theta j (-a51 + a52 \cos 2 \theta j)$, b78 = $ukj \cos \theta j (-a51 + a52 \cos 2 \theta j)$, b78 = $ukj \cos \theta j (-a51 + a52 \cos 2 \theta j)$, b78 = $ukj \cos \theta j (-a51 + a52 \cos 2 \theta j)$, b79